SSC-229

SSC-229

Superconducting Super Collider Laboratory

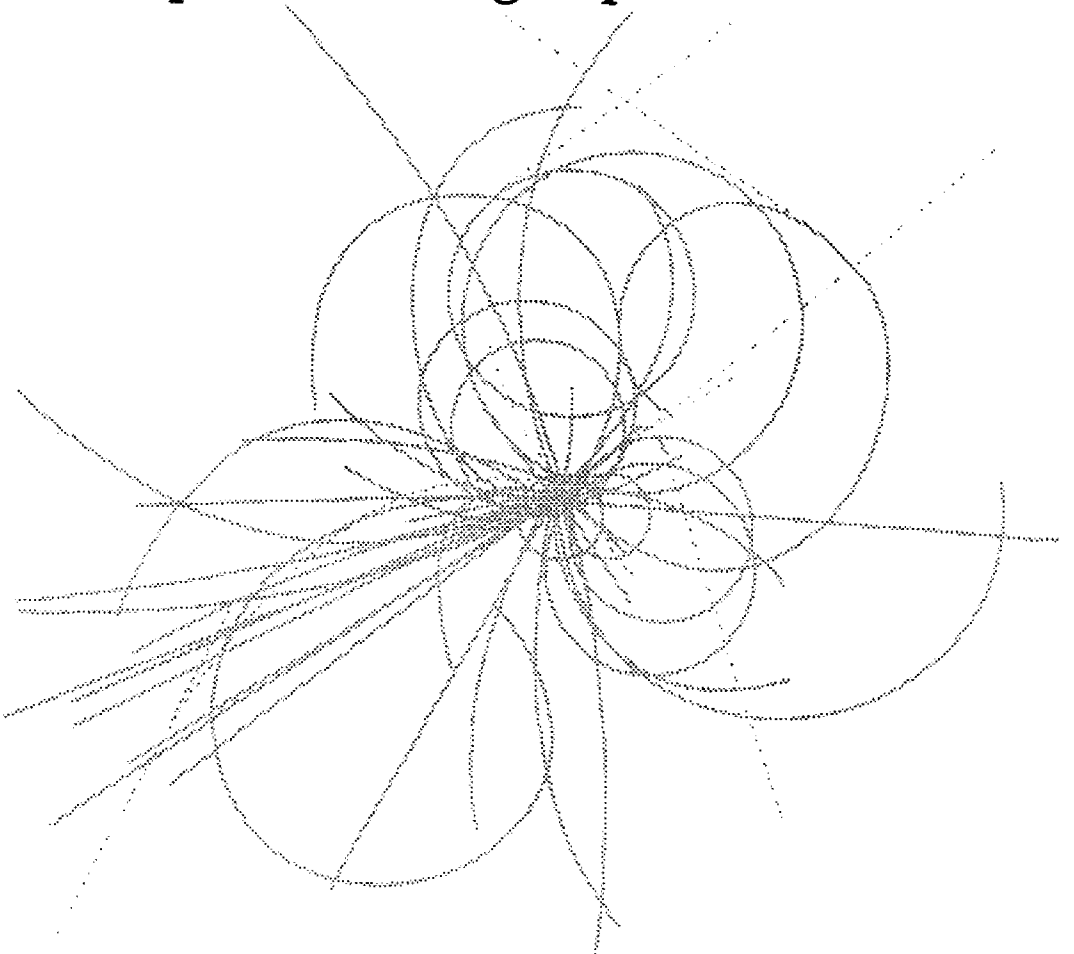

Radiation Levels in SSC Calorimetry

D. Groom
SSC Central Design Group

July 1989

SSC-229

RADIATION LEVELS IN SSC CALORIMETRY*

Don Groom
SSC Central Design Group†

July 1989

* Submitted to the Proceedings of the Workshop on Calorimetry for the Superconducting Supercollider, Tuscaloosa, AL, March 13–17, 1989.

† Operated by the Universitites Research Association for the U.S. Department of Energy

SSC-229
21 July 1989

Radiation Levels in SSC Calorimetry

Donald E. Groom
for the
Task Force on Radiation Levels in the SSC Interaction Regions*
SSC Central Design Group,†
Lawrence Berkeley Laboratory 90-4040, Berkeley CA 94720

Estimates of ionizing dose and neutron fluence have been made for typical SSC detector configurations exposed to radiation from p-p collisions. Using a description of "average events" in conjunction with simulations of secondary processes, it is found that in most cases the ionizing dose (D) or neutron fluence (ϕ) can adequately be expressed as

$$D \text{ (or } \phi) = \frac{A}{r^2 \sin^{\alpha+2}\theta} \ .$$

Here A depends on the process and exposure time, and α is slightly less than unity. For calorimetry r is the distance from the interaction point. Under nominal conditions a calorimeter element 2 m from interaction point and 6° from the beam line is subjected to an annual dose is 0.1 MGy at electromagnetic shower maximum and an annual neutron fluence of $10^{14}\,\mathrm{cm}^{-2}$at hadronic cascade maximum. A detector at an 8 TeV × 8 TeV p-p collider with the same "physics reach" would experience about 27 times as much radiation.

1. Introduction

High energy and high luminosity combine to create a radiation environment for experiments the Superconducting Supercollider (SSC) that is orders of magnitude more severe than at existing accelerators. Radiation problems must be addressed in any serious detector design. Accordingly, an SSC Central Design Group task force was formed to make as quantitative an assessment of the radiation level as is possible in the absence of a specific detector design. In the following we briefly summarize the approach and main results given in the task force report [1].

In contrast to radiation at present colliders, most of the radiation in an SSC interaction region (IR) comes from the 20 TeV on 20 TeV p-p collisions. At the design luminosity, about 10^8 collisions per second occur, and we assume that this luminosity is maintained for 10^7 s out of each year. At this luminosity the beam-beam collisions at each IR contribute (300 hr)$^{-1}$ to the reciprocal of the current lifetime, so collision products strike the detector at a rate equivalent to

---

* F. S. Alsmiller, R. G. Alsmiller, Jr., S. Ban, J. E. Brau, K. W. Edwards, A. Fassò, H. Fesefeldt, T. A. Gabriel , M. G. D. Gilchriese (Chairman), D. E. Groom, H. Hirayama, H. Kowalski, H.W. Kraner, N. V. Mokhov, D. R. Nygren, F. E. Paige, J. Ranft, J. S. Russ, H. Schönbacher, T. Stanev, G. R. Stevenson, A. Van Ginneken, E. M. Wang, R. Wigmans, and T. P. Wilcox, Jr.

† Operated by the Universities Research Association for the U. S. Department of Energy.

the accidental loss of one beam into the apparatus every 6 days. By comparison, beam-gas collisions and expected particle loss contribute very little. Accidental processes such as beam loss during injection are more problematical, but if these are significant the machine cannot operate as planned.

For purposes of this study, the calorimeter has been modeled as a spherical shell extending down to some cutoff angle from the beam line, typically 6°. More distant endcap calorimeters extend the coverage down to some smaller angle. Since all results scale inversely with the distance from the interaction point, the exact geometry is not critical.

An incident hadron produces both an ionizing dose and a neutron fluence in a calorimeter. Backscattered neutrons enter the central cavity, and there might be substantial rear leakage. About a third of the particles from the primary collision are π^0's, so as many photons as hadrons strike the calorimeter. The resulting showers produce an ionizing dose that peaks more sharply and therefore more intensely than does the dose from an electromagnetic cascade.

A very simple approach has been used to describe these processes. In the first place, particle production is described—not particle production in the rare interactions of physics interest, but in the "minimum bias" events that occur 10^{15} times each year. Secondly, the interactions of single hadrons or photons with the detector are described and parameterized as a function of incident energy or momentum. The results are then combined to obtain the desired dose rate or flux. In a few cases "global" calculations have also been made; these corroborate the general approach but raise a few caveats. There are uncertainties in both particle production and in the effects of individual particles, and some of the assumptions are approximate. For example, the transverse size of a cascade is assumed to be small compared with the distances over which the incident flux changes appreciably, an assumption which is certainly not valid very close to the beam line. Uncertainties from all of these sources are such that the results are thought to be dependable to within factors of four or less.

2. Particle production

At least two interaction regions (IRs) at the SSC will have a luminosity of $10^{33}\text{cm}^{-2}\text{s}^{-1}$ with the SSC operating at $\sqrt{s} = 40$ TeV. If the inelastic p-p cross section is 100 mb, the interaction rate in each of these IRs will be 10^8s^{-1}. If the annual average is 1/3 of this luminosity, there will be 10^{15} interactions per year. We take this as our standard input number in making radiation calculations.

This luminosity will obtain with 10^{14} protons in each ring, and so 10^8 s^{-1} implies a $(300\text{ hr})^{-1}$ contribution to the inverse current lifetime. The nominal collision rate is thus equivalent to dumping one beam into the detector every 6 days. It also means that any competing beam-loss mechanism would substantially decrease the beam lifetime and would very likely quench or damage machine components. It is hence reasonable to assume that most of the radiation in a detector

is the result of p-p collisions at the interaction point. This assumption is different than for the present generation of machines.

In calculating radiation effects, we are concerned with "average" collisions rather than the rare collisions with high transverse momentum that are of physics interest. These "minimum bias" events have been studied with the aid of ISAJET [2], PYTHIA [3], and DTUJET [4]. In spite of some theoretical problems, a reasonable extrapolation from lower energies is possible because of the relatively slow variation of the data with $\ln s$. It is possible to write the charged multiplicity in an average event as a function of pseudorapidity (η)* multiplied by a function of the momentum component perpendicular to the beam direction ($p_\perp = p/\sin\theta$).† Moreover, the function of η is constant within about 10% over the entire range covered by a detector:

$$\frac{d^2 N_{\rm ch}}{d\eta dp_\perp} \approx H\, f(p_\perp) \tag{1}$$

Here H is the average height of the pseudorapidity plateau and $f(p_\perp)$ describes the transverse momentum distribution.

Experimental measurements of the central height of the rapidity plateau for charged particle production are shown in Fig. 1. The CDF data are from Ref. 5, and the remaining data and fits are from Ref. 6. The extrapolated height at the SSC energy is about 7.0, and we estimate the average plateau height to be 8% or 10% higher than the central value. On this basis, we take $H = 7.5$ for this study.

Similarly, $\langle p_\perp \rangle$ $(= \int p_\perp f(p_\perp) dp_\perp / \int f(p_\perp) dp_\perp)$ is shown in Fig. 2. A "French curve" extrapolation yields about 0.60 GeV/c at $\sqrt{s} = 40$ TeV.

Several functional forms have been used for $f(p_\perp)$. A function proportional to $p_\perp \exp(-p_\perp/B)$ is usually sufficient, since the "skirt" appearing in the experimental distribution at high $p_\perp$ has little effect in radiation calculations. For most applications the distribution given by Eq. 1 is folded with a single-particle response of the form Np^α, where $0.5 < \alpha < 1.0$. Integration results are changed by less than 10% if realistic forms for $f(p_\perp)$ are replaced by

$$f(p_\perp)\ \big(= f(p/\sin\theta)\big) = \delta(p_\perp - \langle p_\perp \rangle)\ . \tag{2}$$

About half as many π^0's as charged hadrons are produced in the primary collision, with a distribution given by Eq. 1 except with a value for H that is half as large. We therefore assume the same number of (decay) photons as charged particles per rapidity interval, with a momentum distribution having half the mean

* The pseudorapidity $\eta = -\ln\tan\theta/2$ is the same as the rapidity y for $p >> m$ and $\theta >> 1/\gamma$. The identity $\cosh\eta \sin\theta = 1$ is particularly useful for this study.

† More accurately, the momentum distribution $f(p_\perp)$ is independent of the rapidity y. The distinction is important in the central region where p is not large compared with m, but not to the accuracy needed for radiation calculations.

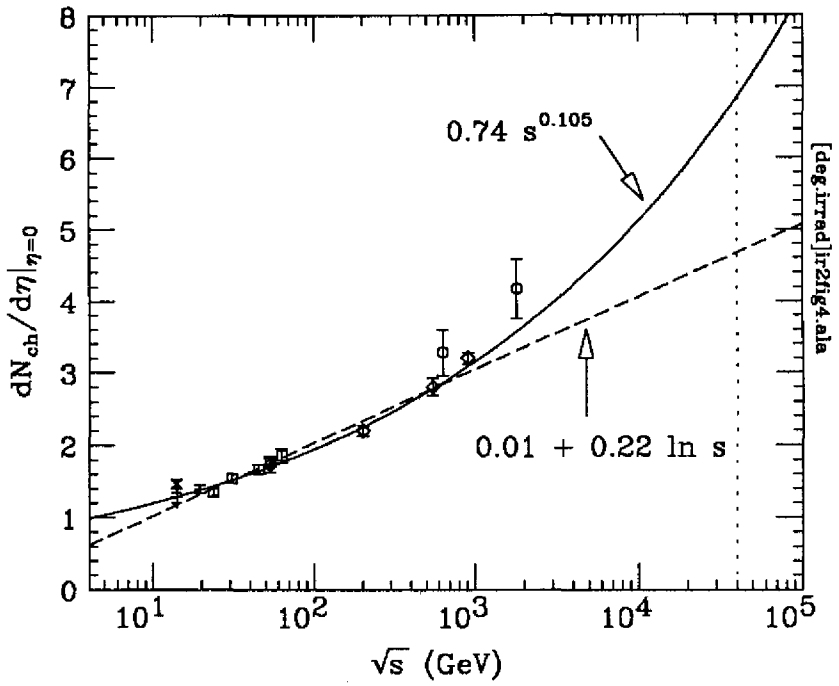

FIG. 1. $dN_{\rm ch}/d\eta|_{\eta=0}$, based on FNAL fixed target (+ and ×), ISR (□), S$\bar{\rm p}$pS (◇), and preliminary CDF (○) data. The CDF points [5] have been added to data taken from Fig. 2 in Alner *et al.* [6], and the two fits shown are to the data exclusive of CDF.

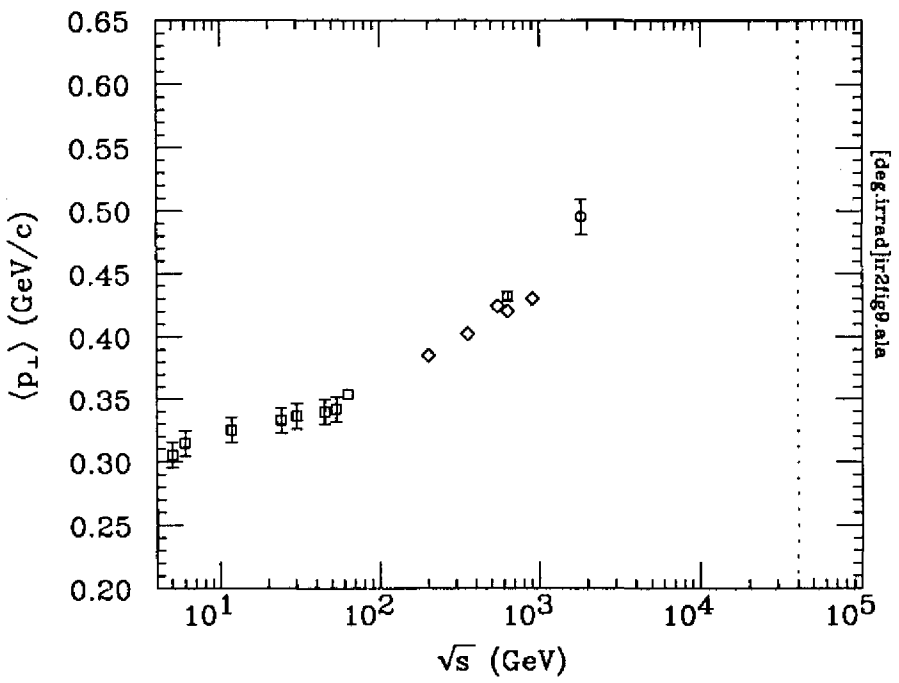

FIG. 2. The variation of the mean value of $p_\perp$ with center of mass energy for the distribution $d^2N_{\rm ch}/dy\,dp_\perp$ for minimum bias events [5]. ISR (□), S$\bar{\rm p}$pS (◇), and CDF (○) results are shown.

value as that for charged hadrons. The effect of the γ-ray decay angle and momentum distributions has not yet been studied in sufficient detail.

Our main conclusions about radiation in calorimeters may be drawn from Eq. 1 alone. $dN_{\rm ch}/d\eta$ is constant, and $d\eta/d\Omega = 1/(2\pi \sin^2\theta)$. Hence, $dN_{\rm ch}/d\Omega$ is a constant divided by $\sin^2\theta$. The mean value of the momentum (or energy) at this angle is $\langle p_\perp \rangle / \sin\theta$. Hence the energy going into unit solid angle is proportional to $1/\sin^3\theta$, and the energy striking unit area a distance r from the interaction point is proportional to $1/(r^2 \sin^3\theta)$. Maximum ionizing dose or maximum neutron fluence is at least roughly proportional to the incident energy density, and so it has the same dependence upon distance and angle. Symbolically, this logic flow is as follows:

$$\left.\begin{array}{l} \dfrac{dN_{\rm ch}}{d\eta} = \text{Const} \\[2ex] \dfrac{d\eta}{d\Omega} = \dfrac{1}{2\pi \sin^2\theta} \end{array}\right\} \left.\begin{array}{l} \dfrac{dN_{\rm ch}}{d\Omega} = \dfrac{\text{Const}}{\sin^2\theta} \\[2ex] E \approx p = \dfrac{p_\perp}{\sin\theta} \end{array}\right\} \left.\begin{array}{l} \dfrac{dE}{d\Omega} = \dfrac{\text{Const}}{\sin^3\theta} \\[2ex] \dfrac{d\Omega}{da} \propto \dfrac{1}{r^2} \end{array}\right\} \begin{array}{l}\text{Neutron fluence} \\ \text{or ionizing dose}\end{array} = \frac{K}{r^2 \sin^3\theta} \tag{3}$$

3. Effect of individual particles

Eq. 3 is insufficient for a number of reasons. In the first place, the constant K must come from Monte Carlo simulations, hopefully supplemented by experimental measurements. Secondly, since showers lengthen with energy the maximum amplitude is not quite proportional to the incident energy density, so that the power of $\sin\theta$ is a little less than three. This is true for both electromagnetic and hadronic cascades. Finally, hadronic activity increases less rapidly than linearly with energy because π^0 production progressively "bleeds off" more and more energy to the electromagnetic channel as the incident energy increases. This has the effect of further reducing the power of $\sin\theta$ for processes such as neutron production. Even in this case, the combined effect is to reduce the exponent to about 2.7, so the above equation still provides guidance. The inverse r^2 dependence remains rigorously true, and provides a serious constraint on detector design.

Monte Carlo programs were used to simulate the results when a single photon or hadron strikes a calorimeter. EGS4 [7] was used for electromagnetic simulations. For incident hadrons, the dose and neutron flux inside, the neutron leakage from the back, and neutron backscatter from the front were calculated, although not always at the same time. Members of the Task Force variously used CASIM [8], FLUKA [9], GHEISHA [10], HETC [11], and MARS [12] for hadronic cascade simulations. With the exception of GHEISHA, these codes do not transport neutrons after their energies fall below some threshold, typically chosen as 50 MeV. For

several problems in which these neutrons were important the codes ANISN [13], MORSE [14], and COG [15] were used.

In a few cases experimental data were also available. The associated errors were quite large because of interpretative problems. For example, neutron flux was sometimes measured using activation techniques, but usually by means of a reaction whose energy threshold is high compared with the neutron energies of interest, e.g. those that can produce dislocation damage in silicon. More and better experimental results are badly needed.

The calorimeters studied ranged from uranium with silicon readout to iron with proportional wire chamber readout. As might be expected, neutron fluxes were highest for uranium with nonhydrogenous readout and lowest for iron with scintillator readout. A very rough comparison of neutron yield for several common configurations is shown in Table 1. The results should be used with considerable caution, since (a) it was not possible to normalize all calculations to the same reference structure and (b) the scatter between different simulations was quite large. A systematic study of this problem would be quite useful.

Table 1

Relative maximum neutron flux and backscattered neutron flux for various calorimeter configurations.

Calorimeter	Relative flux
U-LiqAr or Si	1.0
Pb-LiqAr or Si	0.5
U-Scint.	0.3
Pb-Scint.	0.15

The most commonly modeled calorimeter was a "fine-sampling uranium/scintillator calorimeter," with alternating 3-mm uranium plates and 3-mm scintillator sheets. This calorimeter was taken as a reference standard for the study.

A simple example of single-particle simulation results is shown in Fig. 3, in which the dose at electromagnetic shower maximum is shown as a function of incident photon energy. Power law fits seem to provide adequate fits to such data. The yield cannot increase faster than linearly with E, and a less rapid rise is to be expected because the cascades become longer as the incident energy increases.

A more complicated example is shown in Fig. 4, where the maximum neutron flux in a calorimeter is plotted as a function of incident hadron energy. The results from four simulations and two experiments (shown by the ellipses) are indicated by various letters. Hadronic cascades are more difficult to describe than electromagnetic showers, and the scatter indicates differences between codes. The solid line is drawn by eye, and the dotted lines are shifted from it by factors of two.

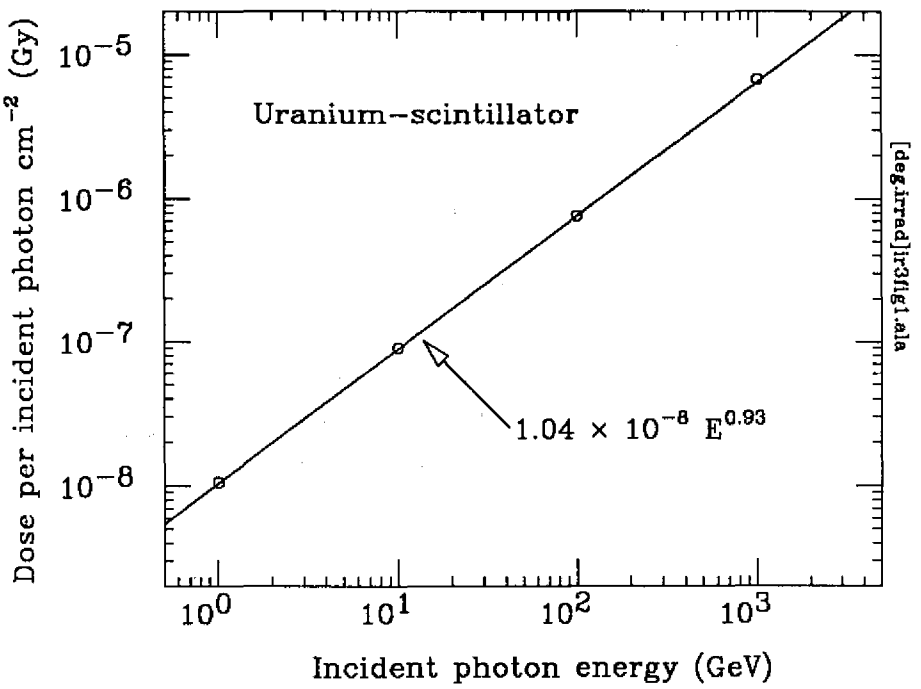

FIG. 3. The maximum electromagnetic dose in Gy for one incident photon per cm^2 in the scintillator of a uranium/scintillator calorimeter as a function of incident photon energy.

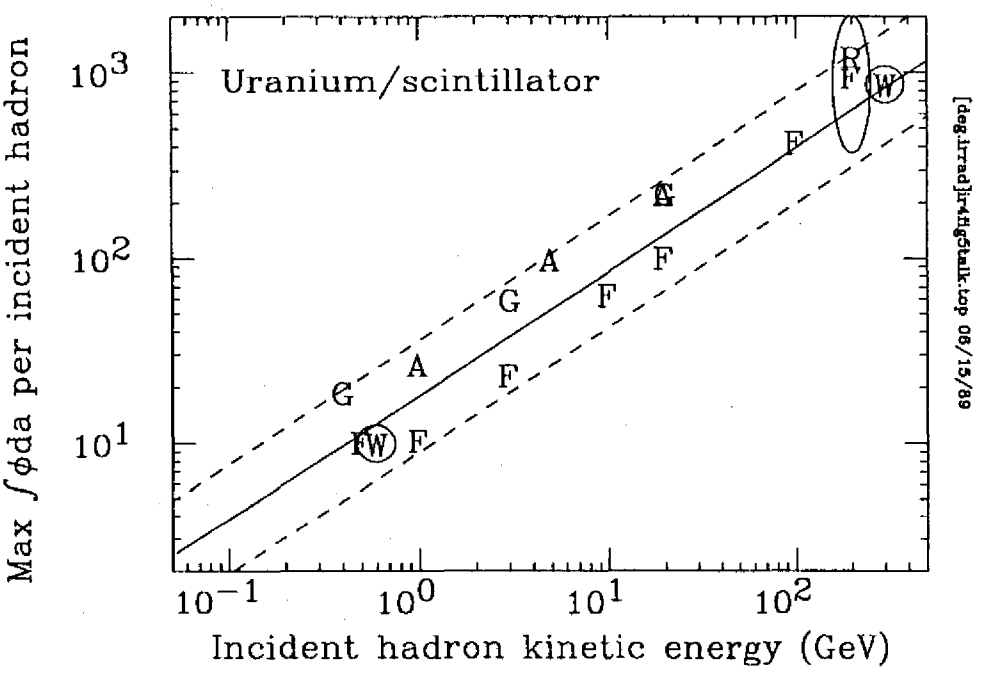

FIG. 4. Summary of selected maximum neutron flux data for a fine-sampling uranium/scintillator calorimeter. The solid curve represents $\int \varphi\, da = 18\,(E_k/(1\,\mathrm{GeV}))^{0.67}$, while the dashed curves are higher and lower by a factor of two. E_k may be replaced by p for practical calculations.

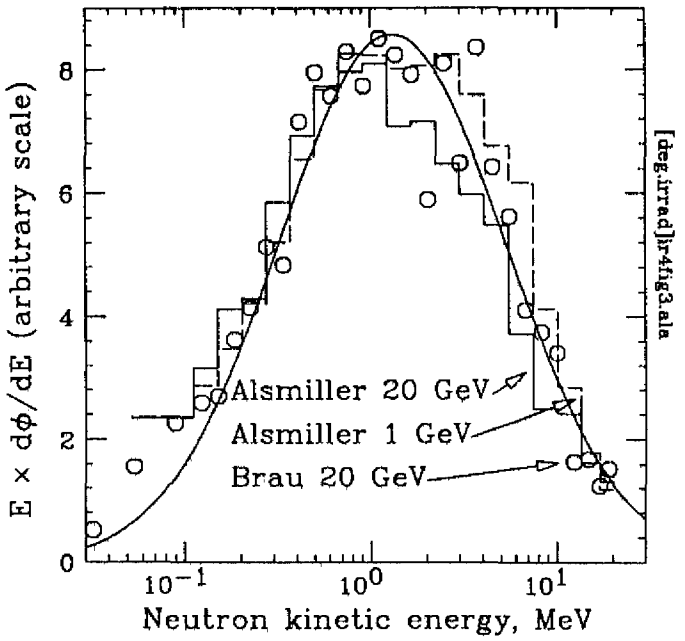

FIG. 5. The spectrum of neutrons backscattered from a uranium/ scintillator calorimeter. The spectra at 1 GeV and 20 GeV were calculated by Alsmiller *et al.* (dashed and solid histograms), and a 20 GeV spectrum calculated by Brau and Gabriel is shown by the circles. Normalizations are chosen so that the peaks coincide. The solid curve is a gaussian in $\ln E_k$.

It is from these and similar data that we have concluded that our results for the response to single incident particles are probably valid to within factors of two.

As a hadronic cascade progresses, charged secondaries tend to "range out," so that below a few tens of MeV the only hadrons of any significance are neutrons. One may think of a "gas" of such neutrons, diffusing away from the shower core, out of the front face of the calorimeter, and out the back. A sampling of calculated spectra for neutrons from the front face is shown in Fig. 5. According to this "leaking gas" model, it is also representative of the neutron spectrum inside the calorimeter, although one might expect a harder spectrum near the shower core. The distribution in the logarithm of the kinetic energy is roughly gaussian, with a maximum at 1.3 MeV and a standard deviation corresponding to a factor of 3.7 from the mean, as shown by the smooth curve in Fig. 5. This "1-MeV" spectrum is characteristic of all processes we have examined. In some situations it is found to be slightly softer (e.g. the neutrons escaping from the Tevatron or SSC dipoles as a result of beam-gas losses [16]) and in some cases slightly harder, but in general most of the neutrons under the peak are above the effective threshold for damaging silicon devices (about 0.15 MeV) and have a silicon damage coefficient close to that for 1-MeV neutrons.

In a few cases neutron transport was extended to thermal energies. The thermal flux is very close to the "1-MeV" flux, and we believe it has little importance in the present context.

4. Results

As discussed in the previous section, the effect (dose, fluence, number of backscattered particles, etc.) of a single particle incident on a calorimeter can usually be parameterized by a power law in its incident momentum. For example, the radially integrated neutron fluence for one incident hadron on a uranium/scintillator calorimeter can be written as

$$\int \varphi da = N_n \, p^\alpha \, dp \tag{4}$$

with $N = 18$ and $\alpha = 0.67$, where p is measured in GeV/c.* This integral is equal to the fluence at the same depth if one particle with momentum p is incident per unit area. The total response at that point may then be found by multiplying by the particle distribution given by Eq. 1 and integrating over momentum. The integral may be carried out over all momenta, or over momenta above a cutoff imposed e.g. by a central solenoid. This has been done using a variety of forms for $f(p_\perp)$. As discussed in Section 2, in the absence of a momentum cutoff accuracy well within the uncertainties in single-particle response is obtained with $f(p_\perp)$ replaced by a δ-function centered at $\langle p_\perp \rangle$. It follows immediately that the response *per rapidity interval* per average p-p collision can be written in the form

$$H \, N \, \langle p_\perp \rangle^\alpha \cosh^\alpha \eta \ , \tag{5}$$

where the single-particle response is $N \, p^\alpha$ and where we have made use of the identity $\sin\theta \cosh\eta = 1$. Since $d\eta/d\Omega = 1/2\pi \sin^2\theta$, the corresponding effect per unit solid angle is proportional to $\langle p_\perp \rangle^\alpha \cosh^{\alpha+2} \eta$.

The flux of particles incident on a detector at a given point scales inversely as the distance from the interaction point. It follows that for a calorimeter,

$$\begin{aligned} \text{Dose or fluence} &= A \, \langle p_\perp \rangle^\alpha \cosh^{\alpha+2} \eta / r^2 \\ &= \frac{A \, \langle p_\perp \rangle^\alpha}{r^2 \sin^{\alpha+2} \theta} \end{aligned} \tag{6}$$

In calorimetric problems ranging from the calculation of neutron fluence to the calculation of dose from electromagnetic cascades, $0.7 < \alpha < 0.9$, so that $\alpha + 2$ is slightly less than three. The same result was obtained by a more general argument in Eq. 3.

As a matter of convenience for presenting results, we have standardized either to an inside radius of 2 m or to a distance of 2 m to the interaction point. However, the scaling of all radiation effects with the inverse square of typical detector dimensions must be kept in mind. The penalties for a compact detector design are obvious.

* Since $p \approx E$ we have been careless in making a distinction between energy and momentum.

We illustrate the results presented in Ref. 1 with two examples. Fig. 6 shows the maximum annual neutron fluence in a uranium/scintillator calorimeter under standard operating conditions. Fig. 7 shows the annual ionizing dose produced by hadrons (solid curve) and photons (dashed curve) under the same conditions. Although photons carry only about half the energy as do the charged particles, the showers peak more sharply and thus have higher maxima. As might be expected, the dose ratio is about the ratio of a nuclear interaction length to a radiation length. A calorimeter is exposed to the highest radiation levels near the electromagnetic shower maximum.

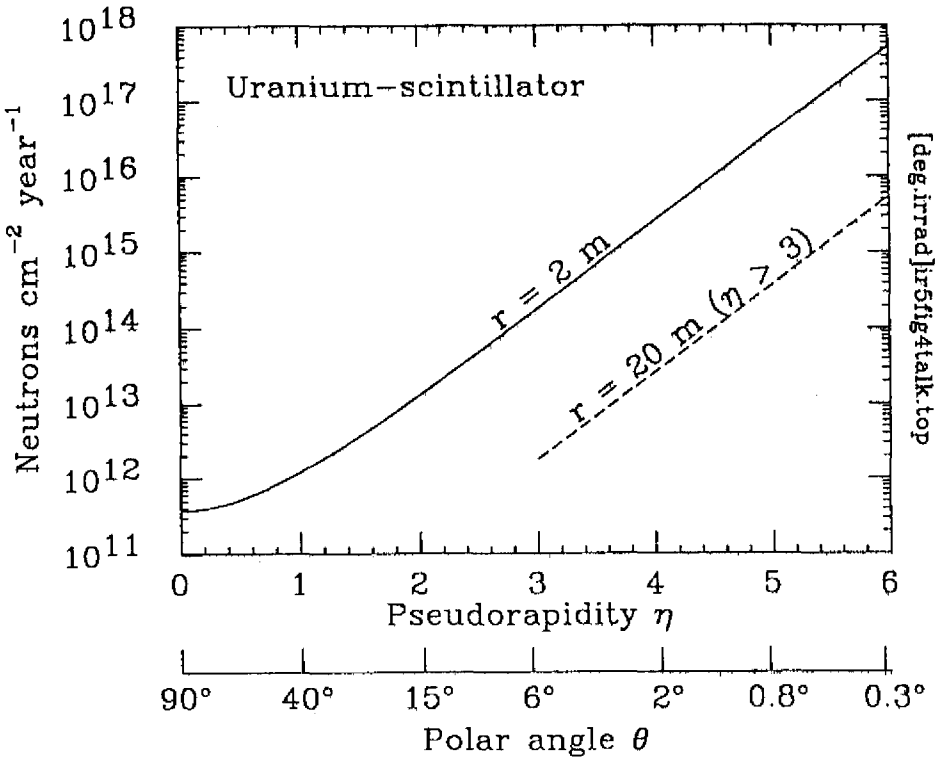

FIG. 6. The maximum neutron flux for a uranium/scintillator calorimeter. The solid curve shows the result assuming the maximum occurs at a radius of 200 cm. Also shown is the result for a radius of 20 m, typical of forward detectors, for rapidity > 3.

5. Application to other hadron colliders

In the context of the approximations summarized in Eqs. 7 and 8, the dose or fluence at any point in a detector at a hadron collider scales as

$$\text{Dose or fluence} \propto \left(\int_T \mathcal{L}\, dt \right) \sigma_{\text{inelastic}}\, H\, \langle p_\perp \rangle^\alpha \ . \tag{7}$$

For comparison purposes we assume the same duty cycle for all colliders and replace the luminosity integral by its nominal value. The factors appearing in Eq. 7 are evaluated in Table 2 for the Tevatron, the high-luminosity version of the proposed large hadron collider (LHC), and the SSC. The exponent α varies

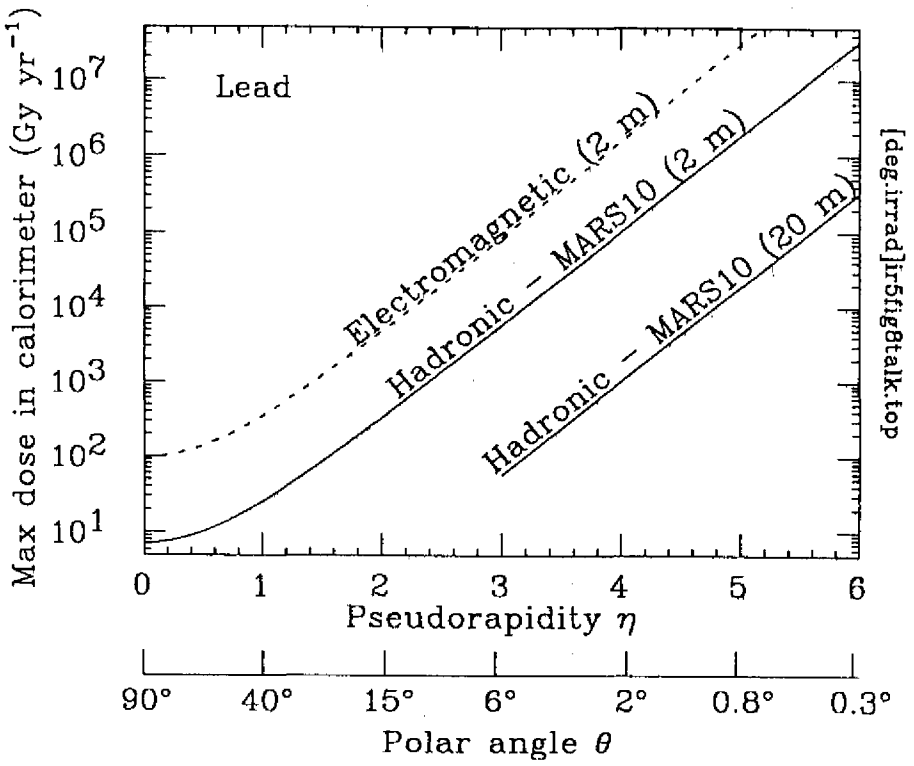

FIG. 7. The maximum hadronic dose as a function of pseudorapidity for a lead sphere, assuming that the maximum dose occurs at the indicated radius. The maximum electromagnetic dose in uranium/scintillator is shown by the dashed line. Since the radiation length, nuclear interaction length, and density are nearly identical for the two materials, dose (but not neutron flux) results may be compared directly.

from 0.5 for neutron backscattering to 0.9 for the maximum electromagnetic and hadronic dose; for scaling purposes we take 0.7 as typical. An inelastic cross section of 100 mb has been adopted for 40 TeV. This value has been roughly scaled with the aid of a fit to existing data to obtain the values given in the Table [17].* The values of H and $\langle p_\perp \rangle$ are obtained from Figs. 1 and 2. The final row gives radiation scale factors, normalized to 1.0 for the SSC. The nominal luminosity given for the Tevatron is fairly arbitrary, but in any case most of the radiation experienced by detectors at the Tevatron collider comes from other sources, such as the main ring.

6. Conclusions

A combination of uncertainties about the inelastic cross section, multiplicity, and mean transverse momentum lead to uncertainties of perhaps a factor of two in our description of particle production at the SSC. Similar uncertainties exist in

* There is recent evidence from cosmic ray measurements at high energies [18] and coulomb-nuclear interference measurements at the $S\bar{p}pS$ [19] that the inelastic cross section at 40 TeV may be substantially larger than 100 mb, perhaps by as much as 50% [20]. We will await Tevatron results before revising any conclusions.

Table 2

A rough comparison of beam-collision induced radiation levels at the Tevatron, SSC, and high-luminosity LHC.

	Tevatron	LHC	SSC
$\sqrt{s}$ (TeV)	1.8	16	40
$\mathcal{L}_{\text{nom}}$ ($\text{cm}^{-2}\text{s}^{-1}$)	2×10^{30}	4×10^{34}	1×10^{33}
$\sigma_{\text{inelastic}}$	59 mb	86 mb	100 mb
H	4.1	6.3	7.5
$\langle p_\perp \rangle$ (GeV/c)	0.46	0.55	0.60
Scale factor	5×10^{-4}	27	1

parameterizing single-particle response. In most cases, estimates of radiation levels in SSC detectors are therefore thought to be valid to within factors ranging from two to four. In certain regions (e.g. very near the beam line) our approximations compromise the accuracy of the results.

The effects of this radiation on the materials used in detectors is discussed elsewhere [21]. It appears likely that with sufficient care in the choice of materials radiation damage will not be the limiting factor in the lifetime of most parts of a large general-purpose detector at the SSC. This qualified statement could not be made if the design luminosity were an order of magnitude higher.

10. References

1. "Report of the Task Force on Radiation Levels in the SSC Interaction Regions," ed. by D. E. Groom, SSC Central Design Group Report SSC-SR-1033 (June 1988).
2. F. E. Paige and S. D. Protopopescu, "ISAJET 5.35, A Monte Carlo Event Generator for p-p and p-$\bar{\text{p}}$ Reactions," ISAJET PAM file; F. E. Paige and S. D. Protopopescu, in *Physics of the Superconducting Supercollider*, ed. by R. Donaldson and J. Marx, p. 320 (Snowmass CO, 1986).
3. H.-U. Bengtsson, Torbjörn Sjöstrand, "The Lund Monte Carlo for Hadronic Processes—PYTHIA version 4.8," LU TP 87-3 (Jan 1987);
   H. U. Bengtsson and T. Sjöstrand, in *Physics of the Superconducting Supercollider*, ed. by R. Donaldson and J. Marx, p. 311 (Snowmass CO, 1986).
4. J. Ranft, P. Aurenche, F. Bopp, A. Capella, K. Hahn, J. Kwiecinski, P. Maire and J. Tran Thanh Van, SSC Central Design Group Report SSC-149 (1987).
5. F. Abe *et al.* (CDF), Phys. Rev. Lett. **61**, 1819 (1988).
6. G. J. Alner *et al.* (UA5), Z. Phys. C **33**, 1-6 (1986).
7. W. R. Nelson, H. Hirayama and D. W. O. Rogers, "The EGS4 Code System," SLAC-265, Stanford Linear Accelerator Center (December 1985).
8. A. Van Ginneken, Fermilab Report FN-272, Fermilab, Batavia, IL, USA (1975).
9. P. A. Aarnio, A. Fassò, H-J. Möhring, J. Ranft and G. R. Stevenson, "FLUKA86 User's Guide," CERN TIS-RP/168 (1986);

P. A. Aarnio, A. Fassò, J. Lindgren, J. Ranft and G. R. Stevenson, "Enhancements to the FLUKA86 Program (FLUKA87)," CERN TIS-RP/190 (1987).

10. H. Fesefeldt, "The Physics of Hadronic Showers—Physics and Applications," RWTH Aachen PITHA 85/02 (1985).
11. R. G. Alsmiller, Jr. *et al.*, "Modifications of the High Energy Transport Code (HETC) and Comparisons with Experimental Results," presented at the ANS Topical Conference on Theory and Practices in Radiation Protection and Shielding, 22-24 April 1987, Knoxville, Tennessee; K. C. Chandler and T. W. Armstrong, "Operating Instructions for the High-Energy Nucleon-Meson Transport Code HETC," Oak Ridge National Laboratory Report ORNL-4744 (1972).
12. N. V. Mokhov, J. D. Cossairt. Nucl. Instrum. Methods, A**244**, 349 (1986);
    N. V. Mokhov, Soviet J. Particles and Nuclei, (Sept.-Oct. 1987), pp. 408-426;
    N. V. Mokhov, "The MARS10 Code System: Inclusive Simulation of Hadronic and Electromagnetic Cascades and Muon Transport," Fermilab Report FN-509 (20 March 1989).
13. W. W. Engle, Jr., "A User's Manual for ANISN, A One-Dimensional Discrete Ordinates Transport Code with Anisotropic Scattering," K-1693, Union Carbide Corporation, Oak Ridge, TN (1967).
14. M. B. Emmett, "The MORSE Monte Carlo Radiation Transport Code System," Oak Ridge National Laboratory Report ORNL-4972 (February 1975).
15. T. P. Wilcox, Jr., E. M. Lent, "COG: A Particle Transport Code Designed to Solve the Boltzman Equation for Deep-Penetration (Shielding) Problems—Volume I, Users Manual," Lawrence Livermore National Laboratory Report M-221-1.
16. T. A. Gabriel, F. S. Alsmiller, R. G. Alsmiller, Jr., B. L Bishop, O. W. Hermann, and D. E. Groom, "Preliminary Simulation of the Neutron Flux Levels in the Fermilab Tunnel and Proposed SSC Tunnel," SSC Central Design Group Report SSC-110 (1987).
17. D. E. Groom, "The Total p-p Cross Section at 40 TeV," SSC Central Design Group Note SSC-N-154 (1986).
18. T. K. Gaisser, U. P. Sukhatme, and G. B. Yodh, Phys. Rev. D**36**, 1350 (1987).
19. UA4 Collaboration, Phys. Lett. **B198**, 583 (1988).
20. M. Block, *Proc. of the 1988 Summer Study on High Energy Physics in the 1990's* (Snowmass CO, to be published).
21. "Radiation Effects at the SSC," ed. by M. G. D. Gilchriese, SSC Central Design Group Report SSC-SR-1035 (June 1988).